Ultrasoft Porous 3D Conductive Dry Electrodes for Electrophysiological Sensing and Myoelectric Control

Shanshan Yao,

Department of Mechanical Engineering, Stony Brook University, Stony Brook, New York 11794, USA

Department of Mechanical and Aerospace Engineering, North Carolina State University, Raleigh, North Carolina 27695, USA

Weixin Zhou,

Department of Mechanical and Aerospace Engineering, North Carolina State University, Raleigh, North Carolina 27695, USA

Robert Hinson,

Joint Department of Biomedical Engineering at University of North Carolina-Chapel Hill and NC State University, Chapel Hill/Raleigh, North Carolina 27599/27695, USA

Penghao Dong,

Department of Mechanical Engineering, Stony Brook University, Stony Brook, New York 11794, USA

Shuang Wu,

Department of Mechanical and Aerospace Engineering, North Carolina State University, Raleigh, North Carolina 27695, USA

Jasmine Ives,

Department of Mechanical Engineering, Stony Brook University, Stony Brook, New York 11794, USA

Xiaogang Hu,

Joint Department of Biomedical Engineering at University of North Carolina-Chapel Hill and NC State University, Chapel Hill/Raleigh, North Carolina 27599/27695, USA

He Huang,

Joint Department of Biomedical Engineering at University of North Carolina-Chapel Hill and NC State University, Chapel Hill/Raleigh, North Carolina 27599/27695, USA

Yong Zhu

Department of Mechanical and Aerospace Engineering, North Carolina State University, Raleigh, North Carolina 27695, USA

Abstract

Corresponding Authors: shanshan.yao@stonybrook.edu; yong_zhu@ncsu.edu.

Biopotential electrodes have found broad applications in health monitoring, human-machine interactions, and rehabilitation. Here, we report the fabrication and applications of ultrasoft breathable dry electrodes that can address several challenges for their long-term wearable applications – skin compatibility, wearability, and long-term stability. The proposed electrodes rely on porous and conductive silver nanowire based nanocomposites as the robust mechanical and electrical interface. The highly conductive and conformable structure eliminates the necessity of conductive gel while establishing a sufficiently low electrode-skin impedance for high-fidelity electrophysiological sensing. The introduction of gas-permeable structures via a simple and scalable method based on sacrificial templates improves breathability and skin compatibility for applications requiring long-term skin contact. Such conformable and breathable dry electrodes allow for efficient and unobtrusive monitoring of heart, muscle, and brain activities. In addition, based on the muscle activities captured by the electrodes and a musculoskeletal model, electromyogram-based neural-machine interfaces were realized, illustrating the great potential for prosthesis control, neurorehabilitation, and virtual reality.

Graphical Abstract
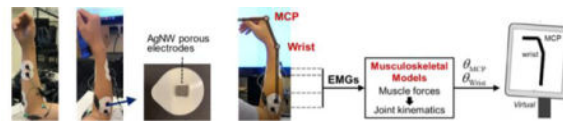
We present the fabrication and potential applications of ultrasoft, breathable, 3D conductive, and gel-free biopotential electrodes. The resulting porous electrodes are skin-like, gas-permeable, and highly conductive, which can form conformable contact with skin and allow for the unobtrusive acquisition of electrophysiological signals. Additionally, based on the muscle activities captured by the electrodes and a musculoskeletal model, electromyogram-based neural-machine interfaces are demonstrated.

Keywords

nanomaterials; dry electrodes; biopotential; electrocardiogram (ECG); electromyogram (EMG); electroencephalogram (EEG)

1. Introduction

Biopotential sensing has been extensively explored in many applications.[1] In personal healthcare, continuous monitoring of biopotential signals, such as electrocardiogram (ECG), electromyogram (EMG), electroencephalogram (EEG), and electrooculogram (EOG), could greatly benefit the clinical physiological tracking and medical treatment.[2] In human-machine interactions, biopotential sensing has been exploited to capture human intents and facilitate natural interactions with smart machines. For example, EMG signals associated with muscle activities and EOG signals associated with eye movements were monitored to drive smart wheelchairs for the disabled.[3] Multimodal EEG/EMG/EOG-based human-machine interfaces were developed to capture hand gestures and eye movements for real-time control of robotic hands.[4] Towards VR/AR applications, EMG[5, 6] and EEG signals[7, 8] were obtained to control virtual avatars, provide timely feedback of

finger movement and facial expressions, and monitor anxiety levels for improved object manipulation and assessment of emotional states and cognitive responses.

In these applications, the most widely used electrodes are pre-gelled and disposable. Several concerns have arisen with pre-gelled electrodes that hinder them from long-term use, including bulkiness, skin irritation, and poor robustness due to gel dehydration.[9] Extensive efforts have been devoted to developing soft dry electrodes that can eliminate the use of conductive gel and minimize interference with natural body movements. Gas permeability, another concern associated with biopotential electrodes, is relatively unexplored but equally important for long-term applications. Existing dry electrodes mainly adopt a solid polymer substrate, which prevents efficient evaporation of sweat and other volatile organic compounds (VOC) from the skin, which provokes skin irritation, signal degradation, and discomfort in long-term applications.[10–12] Porous dry electrodes have recently been fabricated using several processes, such as breath figure based self-assembly,[13] sacrificial templates,[14] bubble blowing,[15] microperforation,[12] and electrospun nanofibers.[16, 17] In these porous electrodes, conductive materials are mostly on the surface of a porous structure, leading to signal degradation over time due to material delamination.[18] Moreover, most electrodes are limited to 2D planar designs with conductive materials on only one side.[11, 12, 19, 20] However, 3D biopotential electrodes with interconnected conductive networks are less explored. 3D electrodes can enable vertical interconnections and substantially improve the integration density for multilayer devices.[21, 22] Additionally, they can eliminate the need for extra interconnects from the skin side (conductive side) and improve the electrode-skin contact.

In this work, we present the fabrication and applications of ultrasoft, 3D conductive, breathable dry electrodes for electrophysiological sensing and neural-machine interface (NMI). The highly conductive and conformable structure enables low electrode-skin impedance and high signal-to-noise ratio (SNR). The good gas permeability and ultralow elastic modulus improve the skin compatibility for applications requiring long-term skin contact. Owing to the 3D interconnected conductive network embedded in a polymer matrix, the electrode remains robust against deformations and sweat during daily activities. The 3D conductivity also facilitates the interconnection to the test unit. The fabricated electrodes are able to acquire high-fidelity electrophysiological signals (i.e., ECG, EMG, EEG) in a truly unobtrusive manner. Additionally, using the developed electrodes and a musculoskeletal model, an EMG-based NMI was realized, where EMG signals corresponding to the flexion/extension of the wrist and metacarpophalangeal (MCP) joints were captured and used as control signals to drive a virtual hand. The EMG-driven control interface can be used for prosthesis control, neurorehabilitation, teleoperation, gaming, and virtual reality.[23]

2. RESULTS AND DISCUSSIONS

2.1. Electrode fabrication by sacrificial templates

Silver nanowires (AgNWs) were used as conductive materials due to their high conductivity and mechanical compliance.[24, 25] Low-cost sacrificial templates, namely interconnected sugar or salt particles, were exploited to assemble AgNW conductive networks into 3D structures. The sacrificial templates were then dissolved to render gas-permeable conductive

electrodes. As schematically illustrated in Figure 1a, sugar or salt particles were mixed with a small amount of water to slightly melt the particles, compressed into the desired shape, and dried to serve as 3D interconnected templates. The slightly melted particles were bonded together (mostly at corners) after drying. The template was then dip-coated in an AgNW/ethanol solution and the solvent was evaporated. The coating and drying process was repeated several times to achieve the desired conductivity. Ecoflex precursors were then poured into the AgNW/template, degassed to allow the liquid Ecoflex to infiltrate into the pores of the template, and cured at room temperature. The cured Ecoflex/AgNW/template was then immersed in hot water to dissolve the sugar or salt. After drying, the completed 3D interconnected porous AgNW/Ecoflex electrodes were then cut into desired shapes.

The final porous electrode is the negative replica of the sugar/salt template with a pore size of a few hundreds of micrometers, depending on the sugar/salt particles size. Since the neighboring particles in the sugar/salt template are connected, the pores in the final porous electrodes are also connected, leading to an open-cell porous structure. AgNWs were randomly arranged and embedded just under the surface of Ecoflex (Figure 1b). This structure has good robustness allowing for long-term use. AgNWs cannot easily detach from Ecoflex scaffolds under repetitive skin abrasion and mechanical deformation during daily activities.

2.2. Characterization of electrode performance

Ideal dry electrodes should be conductive, gas-permeable, conformable to the skin surface, and robust under daily activities. To achieve good signal quality, conformal contact between the electrode and skin and low electrode-skin impedance are required, which further requires low modulus or high work of adhesion at a given electrode thickness.[26] The introduction of 3D porous structures improves the air permeability, enhances the stretchability and deformability, reduces the elastic modulus, but adversely decreases the conductivity of the electrodes. Therefore, the particle size of the sacrificial template and thus the pore size should be optimized to achieve a good balance of air permeability, electrical, and mechanical properties. The conductivity and gas permeability were optimized by employing sugar/salt templates with different particle sizes, which leads to different pore sizes in the final porous structures. Figure 2 summarizes the size distribution and optical images of different sugar/salt particles. Average sizes for table salt, granulated sugar, and sanding sugar are 327.3, 401.4, and 562.1 μm, respectively. Figure 3a reveals that electrodes made from smaller particle sizes achieved similar conductivity after fewer coating-drying cycles. Smaller particle size results in shorter and more ligaments in the porous structure. Therefore, conductive pathways can be more easily established between adjacent ligaments during the dip-coating process in electrodes made from smaller particle sizes.

Conventional flexible and stretchable devices are built upon solid plastic or elastomeric substrates, which leads to a solid barrier against water vapor transpiration and thus prevents skin breathability.[11, 27] Ideally, wearable devices should have sufficient permeability so as not to limit the normal water exchange between skin and ambient.[27] The water vapor transmission rate (WVTR) of the device, defined as the steady flow of water vapor per unit area of the surface in unit time, should be higher than the WVTR for normal skin (8−20

g m^{-2} h^{-1}).[20] WVTR of the porous dry electrode was measured based on the ASTM E96 standard.[13] Briefly, the sample was used to seal a plastic water dish filled with DI water and the weight of the dish was recorded over 48 hours. The water vapor transmission was then calculated from the weight loss. As shown in Figure 3b, the calculated water vapor transmission for porous electrodes increases with pore sizes. Electrodes made from granulated sugar and sanding sugar exhibited a sufficiently high gas permeability (20.9 and 26.8 g m^{-2} h^{-1}, respectively) to allow sweat to emit from the skin.

Taking conductivity and gas permeability together, granulated sugar templates were employed in the following studies to ensure good conductivity and gas permeability. The porosity (*P*) of the porous electrode was estimated by the following expression:[28]

$$P = (1 - \frac{V_{\text{AgNW+Ecoflex}}}{V_{\text{Electrode}}}) \times 100\% \tag{1}$$

where $V_{\text{AgNW+Ecoflex}}$ is the volume of Ecoflex skeleton and embedded AgNWs, which can be calculated from the mass and density of the raw materials used for fabrication. $V_{\text{Electrode}}$ is the macroscopic volume (including the volume of Ecoflex skeleton, embedded AgNWs, and air voids) of the porous electrode and can be obtained from the size of the electrode. The porosity of the electrode made by the granulated sugar template was found to be 67.93 vol% on average.

The elastic modulus of solid Ecoflex was tested to be around 64 kPa (Figure 3c).[29] After introducing porous structures with granulated sugar templates, the elastic modulus of porous Ecoflex was significantly reduced to 7.9 kPa. Further introduction of AgNWs marginally increased the modulus to 12.2 kPa, which is much smaller than that of the epidermis (140 to 600 kPa) and comparable to the dermis (2 to 80 kPa) of the skin.[26] Such low elastic modulus allows for robust electrode-skin contact. Macroscopically, an electrode on the skin can be treated as a film on an epidermis–dermis bilayer substrate.[26] Microscopically, the interfacial contact at the abiotic-biotic interface determines the electrode-skin impedance and signal-to-noise ratio (SNR) for biopotential sensing. For dry surface electrodes, due to the absence of the conductive gel, the gap between the electrode and skin leads to a capacitive behavior at the interface. The measured AC electrode-skin impedance can be modeled by an equivalent circuit shown in Table S1. The resistor R_S represents the total series resistance of the electrode and skin, R_T and Z_{CPE} represent the charge-transfer resistance and double-layer constant-phase element (CPE) at the electrode-skin interface. [16, 30, 31] CPE is introduced to represent the dissipative double-layer capacitance at the electrode-skin interface, considering the nonideal capacitive behavior. The frequency-dependent CPE can be expressed by the following equation:[32]

$$Z_{\text{CPE}} = \frac{1}{Q(j\omega)^n} \tag{2}$$

where $j = \sqrt{-1}$ and ω is the angular frequency. Q indicates the value of the capacitance of the CPE as *n* approaches 1. The parameter n ($0 < n < 1$) represents the capacitance distribution factor.[30, 33] When $n = 1$, the CPE is reduced to the case of an ideal capacitor.

The fitting results for the electrode-skin impedance (Figure 3d) of solid and porous AgNW/Ecoflex electrodes are summarized in Table S1. CPE is defined by two constants, Q and n. By introducing porous structures, the ultrasoft porous AgNW/Ecoflex electrodes can better follow the skin morphology, which reduces the gap between the electrode and skin and maximizes skin contact.[34, 35] As indicated in Table S1, the charge-transfer resistance (R_T) decreased and the double-layer capacitance (CPE-Q) increased, leading to the overall decrease in the electrode-skin impedance (Figure 3d) of the porous electrode. In addition, the CPE-n value increased to 0.80, which is closer to an ideal capacitor. The electrode-skin impedance of the porous AgNW/Ecoflex electrode is much lower than that of AgNW/Ecoflex electrodes without the porous structure, and only marginally higher than that of pre-gelled electrodes. The low electrode-skin impedance of the developed porous electrode is crucial for achieving high SNR in biopotential sensing, to be discussed later. In addition to the method presented in this work, optimized capacitive coupling and minimized electrode-skin impedance were achieved by soft ultra-conformable dry electrodes reported in the literature. Examples include self-adhesive and stretchable conductive polymer electrodes,[36] self-adhesive sub-300 nm gold electrodes,[37] self-adhesive and gas-permeable reinforced polymeric nanofilm electrodes,[38] conformable and robust nanofiber-reinforced nanowire electrodes,[16] and submicron free-standing and breathable hybrid electrodes.[39]

For reliable applications in daily activities that involve skin deformations, skin abrasion, and exposure to sweat, another important factor to consider is the stability. Since the elastic strain range of human skin is around 15% and the skin experiences adverse irreversible effects beyond 30%,[40] the electrodes were therefore tested up to 30% tensile strain (Figure 4a) to warrant typical skin-mountable applications. The fabricated porous electrodes have binary electrical networks: interconnected 3D macroscale porous structures and 2D nanoscale AgNW structures, as illustrated in Figure 4b. While the sliding among 2D AgNW networks is the sensing mechanism for restive strain sensing,[41] this behavior should be suppressed for biopotential sensing to minimize the change in resistance/conductivity under strain. Under deformation, the macropores elongated in the strain direction and shrank in the direction perpendicular to the strain direction. Shape changes in the 3D porous structure can effectively relieve the strain imposed on the 2D AgNW networks.[42, 43] Accordingly, the resistance change under the tensile strain of 30% was found to be around 17%, much smaller than resistance changes (50% to 600%) of 2D AgNW-elastomer composites without 3D porous structures.[44–48] The binary network substantially improved the electromechanical performance.[49] The electromechanical behavior under the compressive strain up to 50% was also tested to evaluate the robustness under compression. The resistance decreased under compression with excellent reversibility (Figure 4c) due to the enhanced electrical contact of AgNW networks, illustrating a piezoresistive effect.[50] Although the focus of this work is on biopotential applications, the response to the compressive strain illustrates the stability under large deformation and its capability for pressure sensing.

In addition to electromechanical robustness, another factor that affects the stability during long-term applications is the resistance to sweat and skin abrasion. As observed in Figure 1b, the majority of AgNW networks were embedded just below the Ecoflex surface, which mitigates the deterioration and delamination of AgNWs under harsh conditions in the presence of sweat and skin abrasion. As demonstrated in Figure 5a, under vigorous and

continuous immersion in the water and sweat for over 7 days, the resistance of the porous AgNW/Ecoflex electrode (after removing the water and sweat for immersion) increased by 8.1% and 20.0%, respectively. To test the long-term performance during daily activities, the electrode was attached to the skin for 7 days and its resistance increased by 10.4% (Figure 5c). For comparison, a control group of electrodes was made by fabricating the porous Ecoflex skeleton first and then dip-coating AgNWs directly on the surface. Since AgNWs were coated without encapsulation, a resistance change of 245 times was seen for 7 days of continuous immersion in the sweat (Figure 5b) and a change of 79 times for 7 days of continuous wear on the skin. The comparison confirmed the improved robustness of the developed electrodes in long-term skin-mountable applications. When peeling off the electrodes after 7 days, no obvious redness and skin irritation were identified (Figure 5d).

Overall, the developed porous dry electrodes can address several challenges faced by the commercial pre-gelled Ag/AgCl electrodes for long-term wearable applications: 1) The electrodes are gel-free and breathable. They rely on porous nanocomposites as the compliant electrical interface to overcome the skin irritation issue of the conductive gel.[51] 2) The electrodes are ultrasoft, stretchable, and compressible, which are significantly less bulky on the skin than the commercial electrodes. 3) The electrodes are robust for long-term use. Due to dehydration of the conductive gel, it is challenging to use commercial pre-gelled electrodes for long-term application. Moreover, when compared with other porous dry electrodes demonstrated in the literature, the electrodes reported here are more robust against long-term wear, owing to the encapsulation of nanomaterials in the polymer matrix. While most other electrodes are limited to 2D planar designs with conductive materials on only one side.[11, 12, 19, 20] the 3D conductive electrode can eliminate extra interconnects on the skin side, facilitate the vertical interconnection, and allow for high integration density for multilayer devices.[21, 22]

2.3. Applications in biopotential sensing

To illustrate different biopotential sensing applications, the biopotential sensing performance in ECG, EEG, and EMG measurements was tested and compared against the gold standard, commercial pre-gelled Ag/AgCl electrodes (Red Dot™, 3M). For ECG sensing, the three-electrode configuration was adopted. Recording and reference electrodes were placed on the right and left forearms and a ground electrode was attached to the right ankle.[52] Commercial pre-gelled electrodes were placed in adjacent for comparison. Owing to the low electrode-skin impedance, the SNR is comparable to that from pre-gelled electrodes (24.51 dB). As shown in Figure 6a, all characteristic peaks corresponding to P, QRS complex, and T waves were clearly discernible, illustrating the high signal quality for ECG sensing. 5 batches of electrodes and 10 electrodes in total were fabricated using granulated sugar as the sacrificial template. The performance of the fabricated electrodes was tested to evaluate the variation of electrodes from batch to batch. As shown in Table S2, the average conductivity of all electrodes after 8 dip-coating cycles was found to be 98.7 ± 87.5 S/cm. All electrodes have very low modulus (13.9 ± 9.6 kPa), at least one order of magnitude lower than that of the epidermis layer of skin. The electrode-skin-impedances, measured on the same person at the same skin location, were 969.2 ± 40.0 kΩ. The average SNR of ECG signals collected

from these electrodes was found to be 24.31 dB, with a standard deviation of 1.29 dB (around 5.3%).

To evaluate the long-term performance during daily activities, the electrodes were worn on the skin for 7 days and only temporarily taken off during bathing or showering. The electrode performance was evaluated for 7-day light physical activities with normal sweating (Figure S1) as well as for 7-day intensive activities with 30-minutes running on the treadmill every day (Figure S2). ECG signals collected on day 0 and day 7 were compared. For light physical activities, the electrode-skin impedance slightly decreased over the 7-day period (Figure S1a), due to the gradually accumulated electrolytes that decrease the electrode-skin impedance.[51, 53] After intensive activities, the electrode-skin impedance decreased obviously (Figure S2a). This can be mainly attributed to the added conductive pathways at the electrode-skin interface because the sweat is ionically conductive.[37] The electrode-skin impedance was largely recovered after the evaporation of the sweat. For both light and intensive daily activities, high-quality ECG can still be obtained from the porous dry AgNW/Ecoflex electrodes after 7 days, with a nearly unchanged SNR (Figures S1b and S2b). The results indicate the capability of the developed electrodes for 7-day biopotential monitoring. Similar stable electrode-skin impedance and/or SNR were observed in other soft dry electrodes, such as carbon nanotube/polymer electrodes (for 7 days)[54] and PEDOT:PSS/graphene electrodes (for 12 hours).[55] In contrast, the electrode-skin impedance increased significantly over time for non-conformable Ag/AgCl/plastic electrodes.[56] Note that the developed porous electrodes are more suitable for long-term applications, owing to their breathability and skin compatibility.

EEG sensing was conducted by a frontal electrode attached to the forehead, an occipital electrode on the scalp at the back of the head, and a ground electrode on the forehead to reduce electrical interference.[57] Two different states of arousal of the cerebral cortex, with EEG signals corresponding to eyes opening and closure, were recorded with both the porous dry AgNW/Ecoflex electrodes and pre-gelled electrodes, as displayed in Figure 6b. EEG signals obtained from the porous electrodes matched that from the gel electrodes, consistent with the high similarity in SNR of signals (6.39 dB for porous electrodes and 6.45 dB for gel electrodes). The alpha rhythm between 8 to 13 Hz is expected in EEG signals when eyes are closed and relaxed.[10, 57] From the power spectrum density (PSD) in Figure 6c, the alpha rhythm at ~10 Hz was clearly visible in both spectrograms. The alpha rhythm disappeared when eyes were opened. These results demonstrate the high-fidelity sensing of the heart, muscle, and brain activities with a similar SNR to the commercial electrodes.

EMG signals were obtained from three electrodes on the forearm muscles. The recording electrode was placed about 3 cm from the elbow, the reference electrode in the middle of the forearm, and the ground electrode near the wrist.[13] During the experiments, the subject was asked to squeeze a hand dynamometer with different grip strengths. Figure 6d presents the EMG activity of forearm muscles for different grip strengths ranging from 5 to 30 N as measured by the hand dynamometer. It is evident that EMG signals captured different muscle activation levels at different grip strengths. The SNR of EMG signals from the porous AgNW/Ecoflex electrodes and pre-gelled electrodes are 24.50 and 25.55 dB, respectively. The difference in SNR for the two sets of data is around 4%. Figure

S2 presents the comparison of EMG signals collected with the developed ultrasoft porous AgNW/Ecoflex electrodes and much stiffer solid AgNW/Ecoflex electrodes without the porous structure. With the porous AgNW/Ecoflex electrodes, the SNR of EMG signals (24.41 dB) is higher than that for AgNW/Ecoflex thin film (17.08 dB), illustrating the superiority of electrodes with low electrode-skin impedance.

2.4. Applications in EMG-based neural-machine interfaces

With the EMG signals collected from the porous electrodes, a wearable and real-time NMI can be developed. The EMG signals associated with hand and wrist movements are employed to control the movement of a virtual hand/wrist. EMG-based NMIs are promising for prosthesis control, neurorehabilitation, teleoperation, gaming, and virtual reality.[23] Here, four pairs of porous electrodes were used to acquire four-channels of surface EMG signals from extrinsic hand- and wrist-muscles (Figure 7a). To facilitate the interconnection between porous electrodes and the test unit, the conductive gel in commercial Ag/AgCl electrodes was removed and replaced with porous dry AgNW/Ecoflex electrodes. Then the silver epoxy was used to electrically connect AgNW/Ecoflex electrodes from the snap button. For long-term real-world applications, this substrate should be replaced with breathable ones to improve comfort. The EMG signals were processed and interpreted using a musculoskeletal model, as illustrated in Figure 7b.

To capture hand and wrist movements, four muscles of interest were identified via palpation and their anatomic locations: The extensor carpi radialis longus (ECRL), extensor digitorum (ED), flexor carpi radialis (FCR), and flexor digitorum superficialis (FDS).[58] Contractions of ECRL and FCR elicit extension and flexion of the wrist joint, respectively. Contractions of ED and FDS elicit extension and flexion of the metacarpophalangeal (MCP) joint, respectively. Porous AgNW/Ecoflex electrodes were placed over the targeted muscles, and a reference electrode was placed over the subject's right clavicle. The electrodes were then connected to a preamplifier and an EMG acquisition system.

Real-time EMG signals were interpreted with a musculoskeletal model to estimate the wrist and MCP joints' flexion/extension angles.[59] Magnitudes of EMG envelopes were normalized by the maximum EMG signal obtained during a maximum voluntary contraction (MVC) of each muscle. The level of muscle activation (ranging from 0% to 100% in value) was estimated by averaging the EMG envelope. In the musculoskeletal model-based EMG interface, each of the four muscles of interest was modeled as a Hill-type actuator with contractile elements and parallel elastic elements.[60] The EMG data were then used to activate the muscle models for force production. The musculoskeletal model used the estimated muscle forces to compute the joint torques and then estimate the joint kinematics via forward dynamic simulation. A more detailed description of the EMG-driven musculoskeletal model can be found in our previous publications.[59, 61] The outputs of the EMG-driven musculoskeletal model (i.e., wrist and MCP flexion/extension joint angles) were used as the control signal to drive a 2-DOF planar stick figure hand/wrist in the virtual environment. The two joints in the virtual hand/wrist correspond to the wrist and MCP, respectively. The posture of the virtual hand replicates the same DOFs as the musculoskeletal model. Before the posture matching task, linear gains were manually

adjusted to scale inputs (EMG) and outputs (joint angles) so the subject could reach a neutral virtual hand posture while relaxed and could comfortably reach all desired targets of the virtual hand.

To illustrate applications of the developed EMG-based prosthesis control, the subject was asked to perform a posture matching task that mimics the motor control requirement of real-world grasping tasks. Specifically, the subject was asked to use muscle activities (manifested in the EMG signals) to control the virtual hand/wrist in order to match the target postures displayed on the computer screen. During the experiment, both the target hand posture and the virtual hand/wrist being controlled by the subject were displayed on the computer screen. If the virtual hand was held within 5 degrees of the target posture (for both joints), the virtual hand turned green to provide visual feedback. The posture was considered successfully matched if the virtual hand was held within 5 degrees of the target posture for 0.5 seconds consecutively. With the real-time EMG interface, the subject successfully utilized the muscle activities to control the virtual hand/wrist and match the target postures, as demonstrated in Figure 7c and Supplementary Movies. Simultaneous multi-joint control of wrist and finger movements in real-time was realized. The success rate of the posture matching task was 96% among 50 trials with an average matching time of 17.4 s. Toward real applications, this posture matching task represents an effective platform to test and train users' abilities to control myoelectric prostheses.[62]

3. CONCLUSIONS

In summary, fabrication and potential applications of ultrasoft, breathable, 3D conductive, and gel-free biopotential electrodes were presented. Water-soluble sacrificial templates and dip-coating process were used to assemble conductive AgNW networks into 3D interconnected porous structures. The fabrication method is simple, economical, and scalable. The resulting porous electrodes are skin-like, gas-permeable, and highly conductive, which can form conformable contact with skin and establish a low electrode-skin impedance. The gel-free and breathable nature addressed skin compatibility concerns with existing pre-gelled electrodes. Furthermore, the electrodes are reliable for daily use. The superior signal quality, improved skin compatibility, and good robustness make them well suited for long-term monitoring. All these features allow for the accurate and unobtrusive acquisition of ECG/EMG/EEG signals. Based on the real-time tracking of EMG signals and the developed musculoskeletal model for interpreting hand/wrist kinematics, an EMG-drive NMI for driving the virtual hand/wrist towards prosthesis control was demonstrated.

4. METHODS

Fabrication of sacrificial templates:

Sacrificial sugar or salt templates were made by mixing sugar/salt particles and DI water in a square petri dish with a weight ratio of 40 : 1. The mixture was then pressed into a disk and heated to remove the added water. This way, sugar/salt templates were made with particles connected at the corner. The liquid is allowed to penetrate in the gap among particles.

Fabrication of porous dry electrodes:

AgNWs were synthesized using a modified polyol method[63] and dispersed into ethanol to achieve a concentration of 1 mg/ml. The sacrificial template was dipped into the AgNW/ ethanol solution followed by evaporating the ethanol at 60 °C for 30 min. The coating and drying process was repeated until the desired conductivity was achieved. Precursors of Ecoflex 0030 (Smooth-On, Inc.) were mixed with a weight ratio of part A to part B of 1 : 1, degassed in a vacuum oven to remove the entrapped air bubbles, and poured over the AgNW coated sugar/salt templates. The petri dish was put inside the vacuum chamber to facilitate the penetration of liquid Ecoflex into the template. The liquid Ecoflex was cured at room temperature for 6 hours to solidify the silicone. The cured Ecoflex/AgNW/template was then immersed in the DI water at a temperature of 60 °C to dissolve the sugar/salt template and generate the porous structure. Finally, the fabricated Ecoflex/AgNW porous structure was dried and cut into the desired shape.

Characterization:

Microstructures of the porous electrode were obtained by optical microscopy (ECLIPSE LV150N, Nikon) and scanning electron microscopy (SEM, Quanta 3D FEG, FEI). Stress-strain curves were obtained using a mechanical stage (DTS Company). The resistance was measured using a digital multimeter (34401A, Agilent). The water vapor transmission of the conductive porous electrode was measured based on the ASTM E96 standard. Briefly, a plastic dish filled with DI water was sealed with a sample. The bottle was placed in a chamber with the mass of the bottle measured every 6 hours. The water vapor transmission was calculated based on the weight loss of water per hour and the area of the sample. The electrode-skin impedance was measured by placing a pair of electrodes 3 cm apart on the forearm. The electrodes were connected directly to a potentiostat (Reference 600, Gamry Instruments) to obtain the impedance at frequencies between 0.1 to 10 kHz. Electrochemical impedance spectroscopy fitting was performed using the EIS Spectrum Analyzer software. For ECG measurements, the three-electrode configuration was adopted. Recording and reference electrodes were placed on the right and left forearm and a ground electrode was attached to the right ankle.[52] For EMG measurements, three electrodes were placed on the forearm muscles, with the recording electrode placed about 3 cm from the elbow, the reference electrode in the middle of the forearm, and the ground electrode near the wrist. [13] For EEG measurements, a frontal electrode was attached to the forehead, an occipital electrode on the scalp at the back of the head, and a ground electrode on the forehead to reduce electrical interference.[57] ECG, EMG, and EEG signals were collected using a bioamp and a data acquisition system (PowerLab 4/26, ADInstruments) with a sampling rate of 1 kHz.

Signal processing of biopotential signals for electrode characterization:

The collected raw signals from the data acquisition system (PowerLab 4/26, ADInstruments, sampling rate: 1 kHz) were band-pass filtered between 0.3 and 100 Hz (ECG signals), 10 and 2000 Hz (EMG signals), and 0.3 and 50 Hz (EEG signals), respectively. A 60 Hz notch filter was also applied to all signals to remove the power line interference. The SNR of ECG, EMG, and EEG signals were calculated using the following equation:[52]

$$SNR_{\text{dB}} = 10\log_{10}(\frac{A_{\text{signal}}}{A_{\text{noise}}})^2 = 20\log_{10}(\frac{A_{\text{signal}}}{A_{\text{noise}}})$$

where A_{signal} is the root mean square of the biopotential signals (i.e., ECG/EMG/EEG signals in this study), A_{noise} is the root mean square of the noise collected in the settling trials (when the subjects are at rest).

Myoelectric control:

The experimental protocol was approved by the University of North Carolina at Chapel Hill Institutional Review Board. The subject was instructed to hold their right arm in a neutral posture, with the elbow flexed at 90 degrees and the palm facing toward their midline. The four muscles of interest were identified via palpation and their anatomic locations.[58] EMG electrodes were placed over the targeted muscles and a reference electrode was placed over the right clavicle. The electrodes were then connected to a preamplifier (MA-420, Motion Lab Systems, Inc., LA) that band-pass filtered the signals between 10 and 2 kHz with a pass-band gain of 20. The preamplifier fed into an EMG acquisition system (MA-300, Motion Lab Systems, Inc., LA) with an anti-aliasing filter with a cut-off frequency of 450 Hz. The EMG signals were sampled at 1 kHz using a data acquisition system (USB-1616HS-BNC, Measurement Computing Corporation, Norton, MA). The digitized EMG signals were streamed and stored into the computer in 100 ms windows. The most recent 2 seconds of the acquired raw EMG data were high-pass filtered with a 4th-order Butterworth zero-lag digital filter with a cutoff frequency at 40 Hz, rectified, and then low pass filtered again a 4th-order Butterworth zero-lag digital filter with the cutoff frequency at 5 Hz. The processed data captured the envelope of EMG signals. The EMG envelope was further downsampled to 100 Hz. The magnitudes of the EMG envelopes were normalized by the maximum EMG signal obtained during a maximum voluntary contraction (MVC) of each muscle. We estimated the level of muscle activation in each channel by averaging the EMG envelope from the most recent 70 ms (7 most recent envelope samples). The muscle activations were input to the musculoskeletal model to estimate muscle forces and joint torques which were used in forward dynamic calculations to estimate wrist and MCP joint angles. The displayed joint angles of the virtual hand were updated every 50 ms (i.e., the virtual hand control rate was 20 Hz).

Statistical Analysis:

All results presented were averaged among at least three measurements and expressed as the mean or mean ± SD. Student's t-test or ANOVA were utilized to determine statistical significance between datasets. A P value < 0.05 was considered to be statistically significant.

Supplementary Material

Refer to Web version on PubMed Central for supplementary material.

Acknowledgements

References

[1]. Wu H, Yang G, Zhu K, Liu S, Guo W, Jiang Z, Li Z, Adv. Sci 2021, 8, 2001938.

[2]. Chi YM, Jung T-P, Cauwenberghs G, IEEE Rev. Biomed. Eng 2010, 3, 106. [PubMed: 22275204]

[3]. Kaur A, J. Med. Eng. Technol 2021, 45, 61. [PubMed: 33302770]

[4]. Zhang J, Wang B, Zhang C, Xiao Y, Wang MY, Front. Neurorobot 2019, 13, 7. [PubMed: 30983986]

[5]. Dwivedi A, Kwon Y, Liarokapis M, in 2020 IEEE International Conference on Systems, Man, and Cybernetics, IEEE.

[6]. Mavridou I, Seiss E, Hamedi M, Balaguer-Ballester E, Nduka C, in 12th International Conference on Disability, Virtual Reality and Associated Technologies (ICDVRAT 2018).

[7]. Tarrant J, Viczko J, Cope H, Front. Psychol 2018, 9, 1280. [PubMed: 30087642]

[8]. Lin C-T, Chung I-F, Ko L-W, Chen Y-C, Liang S-F, Duann J-R, IEEE. Trans. Biomed 2007, 54, 1349.

[9]. Yao S, Zhu Y, JOM 2016, 68, 1145.

[10]. Kabiri Ameri S, Ho R, Jang H, Tao L, Wang Y, Wang L, Schnyer DM, Akinwande D, Lu N, ACS Nano 2017, 11, 7634. [PubMed: 28719739]

[11]. Miyamoto A, Lee S, Cooray NF, Lee S, Mori M, Matsuhisa N, Jin H, Yoda L, Yokota T, Itoh A, Nat. Nanotechnol 2017, 12, 907. [PubMed: 28737748]

[12]. Tian L, Zimmerman B, Akhtar A, Yu KJ, Moore M, Wu J, Larsen RJ, Lee JW, Li J, Liu Y, Metzger B, Qu S, Guo X, Mathewson KE, Fan JA, Cornman J, Fatina M, Xie Z, Ma Y, Zhang J, Zhang Y, Dolcos F, Fabiani M, Gratton G, Bretl T, Hargrove LJ, Braun PV, Huang Y, Rogers JA, Nat. Biomed. Eng 2019, 3, 194. [PubMed: 30948811]

[13]. Zhou W, Yao S, Wang H, Du Q, Ma Y, Zhu Y, ACS Nano 2020, 14, 5798. [PubMed: 32347707]

[14]. Sun B, McCay RN, Goswami S, Xu Y, Zhang C, Ling Y, Lin J, Yan Z, Adv. Mater 2018, 30, 1804327.

[15]. Yang X, Li L, Wang S, Lu Q, Bai Y, Sun F, Li T, Li Y, Wang Z, Zhao Y, Adv. Electron. Mater 2020, 6, 2000306.

[16]. Liu L, Li HY, Fan YJ, Chen YH, Kuang SY, Li ZB, Wang ZL, Zhu G, Small 2019, 15, 1900755.

[17]. Wang Y, Wang J, Cao S, Kong D, J. Mater. Chem. C 2019, 7, 9748.

[18]. Davoodi E, Montazerian H, Haghniaz R, Rashidi A, Ahadian S, Sheikhi A, Chen J, Khademhosseini A, Milani AS, Hoorfar M, Toyserkani E, ACS Nano 2020, 14, 1520. [PubMed: 31904931]

[19]. Chen Y, Lu B, Chen Y, Feng X, Sci. Rep 2015, 5, 1.

[20]. Chae H, Kwon H-J, Kim Y-K, Won Y, Kim D, Park H-J, Kim S, Gandla S, ACS Appl. Mater. Interfaces 2019, 11, 28387. [PubMed: 31294964]

[21]. Gannarapu A, Gozen BA, Adv. Mater. Technol 2016, 1, 1600047.

[22]. Liang S, Li Y, Yang J, Zhang J, He C, Liu Y, Zhou X, Adv. Mater. Technol 2016, 1, 1600117.

[23]. Crouch DL, Pan L, Filer W, Stallings JW, Huang H, IEEE Trans. Neural Syst. Rehabilitation Eng 2018, 26, 1735.

[24]. Yao S, Yang J, Poblete FR, Hu X, Zhu Y, ACS Appl. Mater. Interfaces 2019, 11, 31028. [PubMed: 31373192]

[25]. Yao S, Myers A, Malhotra A, Lin F, Bozkurt A, Muth JF, Zhu Y, Adv. Healthc. Mater 2017, 6, 1601159.

[26]. Kim D-H, Lu N, Ma R, Kim Y-S, Kim R-H, Wang S, Wu J, Won SM, Tao H, Islam A, Yu KJ, Kim T.-i., Chowdhury R, Ying M, Xu L, Li M, Chung H-J, Keum H, McCormick M, Liu P,

Zhang Y-W, Omenetto FG, Huang Y, Coleman T, Rogers JA, Science 2011, 333, 838. [PubMed: 21836009]

[27]. Ferrari LM, Keller K, Burtscher B, Greco F, Multifunct. Mater 2020, 3, 032003.

[28]. Chen F, Lu Y, Liu X, Song J, He G, Tiwari MK, Carmalt CJ, Parkin IP, Adv. Funct. Mater 2017, 27, 1702926.

[29]. Smooth-On Inc., "Ecoflex™ Series Super-Soft, Addition Cure Silicone Rubbers", 2019.

[30]. Li G, Wang S, Duan YY, Sens. Actuators B Chem 2018, 277, 250.

[31]. Zhou H, Lu Y, Chen W, Wu Z, Zou H, Krundel L, Li G, Sensors 2015, 15, 17241. [PubMed: 26193273]

[32]. Rubinson JF, Kayinamura YP, Chem. Soc. Rev 2009, 38, 3339. [PubMed: 20449053]

[33]. Wang K, Parekh U, Pailla T, Garudadri H, Gilja V, Ng TN, Adv. Healthc. Mater 2017, 6, 1700552.

[34]. Jeong JW, Yeo WH, Akhtar A, Norton JJ, Kwack YJ, Li S, Jung SY, Su Y, Lee W, Xia J, Adv. Mater 2013, 25, 6839. [PubMed: 24327417]

[35]. Yeo WH, Kim YS, Lee J, Ameen A, Shi L, Li M, Wang S, Ma R, Jin SH, Kang Z, Adv. Mater 2013, 25, 2773. [PubMed: 23440975]

[36]. Zhang L, Kumar KS, He H, Cai CJ, He X, Gao H, Yue S, Li C, Seet RC-S, Ren H, Nat. Commun 2020, 11, 1. [PubMed: 31911652]

[37]. Nawrocki RA, Jin H, Lee S, Yokota T, Sekino M, Someya T, Adv. Funct. Mater 2018, 28, 1803279.

[38]. Wang Y, Lee S, Wang H, Jiang Z, Jimbo Y, Wang C, Wang B, Kim JJ, Koizumi M, Yokota T, Proc. Natl. Acad. Sci 2021, 118.

[39]. Fang Y, Li Y, Li Y, Ding M, Xie J, Hu B, ACS Appl. Mater. Interfaces 2020, 12, 23689. [PubMed: 32364375]

[40]. Webb RC, Bonifas AP, Behnaz A, Zhang Y, Yu KJ, Cheng H, Shi M, Bian Z, Liu Z, Kim Y-S, Yeo W-H, Park JS, Song J, Li Y, Huang Y, Gorbach AM, Rogers JA, Nat. Mater 2013, 12, 938. [PubMed: 24037122]

[41]. Amjadi M, Kyung KU, Park I, Sitti M, Adv. Funct. Mater 2016, 26, 1678.

[42]. Ge J, Yao HB, Wang X, Ye YD, Wang JL, Wu ZY, Liu JW, Fan FJ, Gao HL, Zhang CL, Angew. Chem. Int. Ed 2013, 52, 1654.

[43]. Gao HL, Xu L, Long F, Pan Z, Du YX, Lu Y, Ge J, Yu SH, Angew. Chem 2014, 126, 4649.

[44]. Lee H, Seong B, Moon H, Byun D, RSC Adv. 2015, 5, 28379.

[45]. Xu F, Zhu Y, Adv. Mater 2012, 24, 5117. [PubMed: 22786752]

[46]. Cai L, Zhang S, Zhang Y, Li J, Miao J, Wang Q, Yu Z, Wang C, Adv. Mater. Technol 2018, 3, 1700232.

[47]. Amjadi M, Pichitpajongkit A, Lee S, Ryu S, Park I, ACS Nano 2014, 8, 5154. [PubMed: 24749972]

[48]. Wang R, Xu W, Shen W, Shi X, Huang J, Song W, Inorg. Chem. Front 2019, 6, 3119.

[49]. Zhu C-H, Li L-M, Wang J-H, Wu Y-P, Liu Y, RSC Adv. 2017, 7, 51.

[50]. Ding Y, Yang J, Tolle CR, Zhu Z, ACS Appl. Mater. Interfaces 2018, 10, 16077. [PubMed: 29651841]

[51]. Meziane N, Webster J, Attari M, Nimunkar A, Physiol. Meas 2013, 34, R47. [PubMed: 24137716]

[52]. Myers AC, Huang H, Zhu Y, RSC Adv. 2015, 5, 11627.

[53]. Searle A, Kirkup L, Physiol. Meas 2000, 21, 271. [PubMed: 10847194]

[54]. Jung H-C, Moon J-H, Baek D-H, Lee J-H, Choi Y-Y, Hong J-S, Lee S-H, IEEE. Trans. Biomed 2012, 59, 1472.

[55]. Zhao Y, Zhang S, Yu T, Zhang Y, Ye G, Cui H, He C, Jiang W, Zhai Y, Lu C, Nat. Commun 2021, 12, 1. [PubMed: 33397941]

[56]. Li G, Wang S, Duan YY, Sens. Actuators B Chem 2017, 241, 1244.

[57]. ADInstruments, "Electroencephalography Student Protocol", 2010.

[58]. Delagi E, Perotto A, Anatomic Guide for the Electromyographer—The Limbs, Thomas, Springfield, IL 1980.

[59]. Pan L, Crouch DL, Huang H, IEEE Trans. Neural Syst. Rehabilitation Eng 2018, 26, 1435.

[60]. Winters JM, in Multiple Systems: Biomechanics and Movement Organization, (Eds: Winters JM, Woo SL-Y), Springer, New York, NY 1990, Ch.

[61]. Crouch DL, Huang H, J. Biomech 2016, 49, 3901. [PubMed: 27814972]

[62]. Simon AM, Hargrove LJ, Lock BA, Kuiken TA, J. Rehabil. Res. Dev 2011, 48, 619. [PubMed: 21938650]

[63]. Huang Q, Zhu Y, Sci. Rep 2018, 8, 1. [PubMed: 29311619]

Author Manuscript

Author Manuscript

Author Manuscript

Author Manuscript
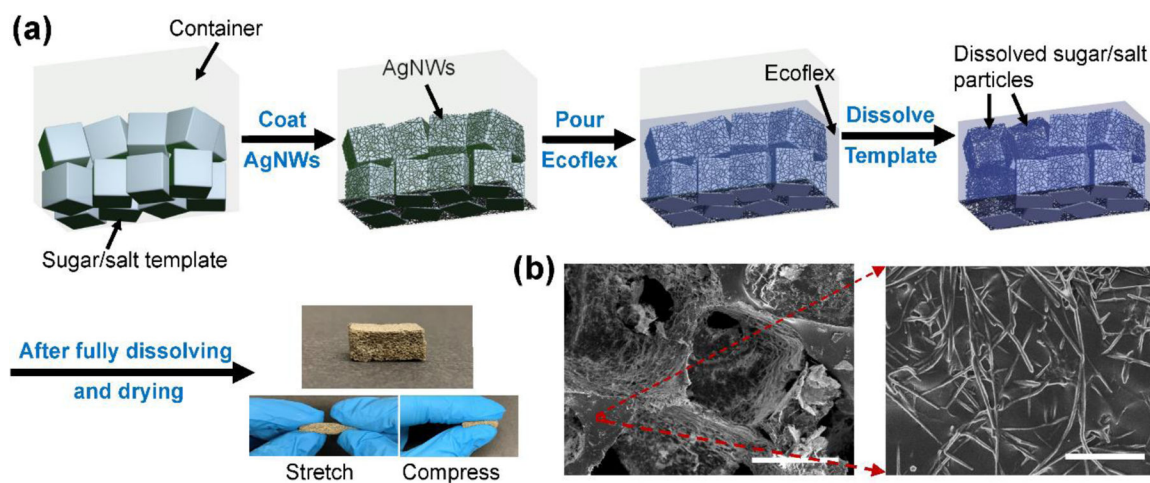
Figure 1.
Fabrication of electrodes using sacrificial templates. (a) Schematic illustration and photographs of porous dry AgNW/Ecoflex electrodes. (b) SEM images of the AgNW/Ecoflex electrode. Scale bars: 400 μm (left) and 2 μm (right).
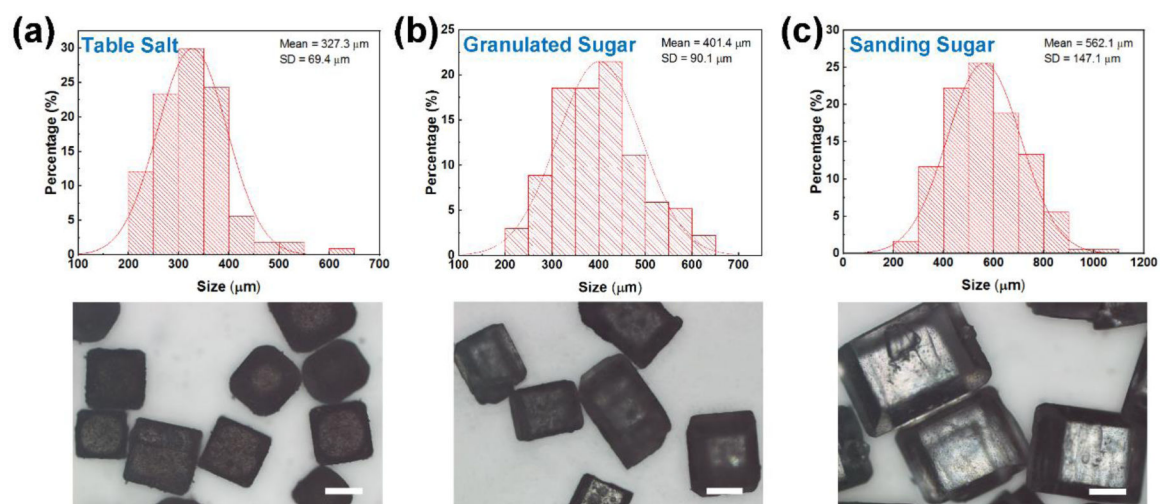
Figure 2.
Size of different sacrificial templates. Size distributions (top) and optical images (bottom) of table salt, granulated sugar, and sanding sugar particles. Scale bars: 200 μm.
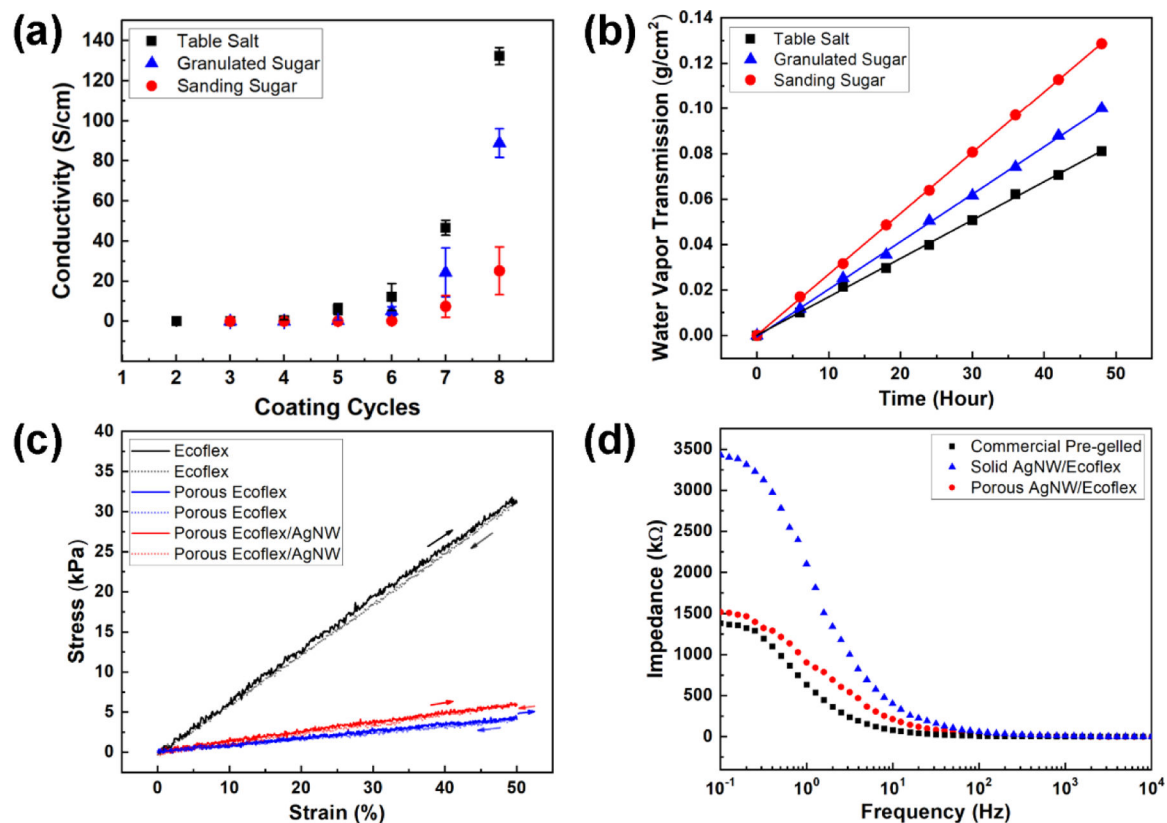
Figure 3.
Characterization of porous dry electrodes. (a) Conductivity as a function of dip-coating cycles for electrodes made from different sacrificial templates. (b) WVTRs for electrodes made from different sacrificial templates. (c) Stress-strain curves for Ecoflex, porous Ecoflex, and AgNW embedded porous Ecoflex. (d) Electrode-skin impedance acquired from commercial pre-gelled Ag/AgCl electrodes, solid AgNW/Ecoflex electrodes, and porous dry AgNW/Ecoflex electrodes.
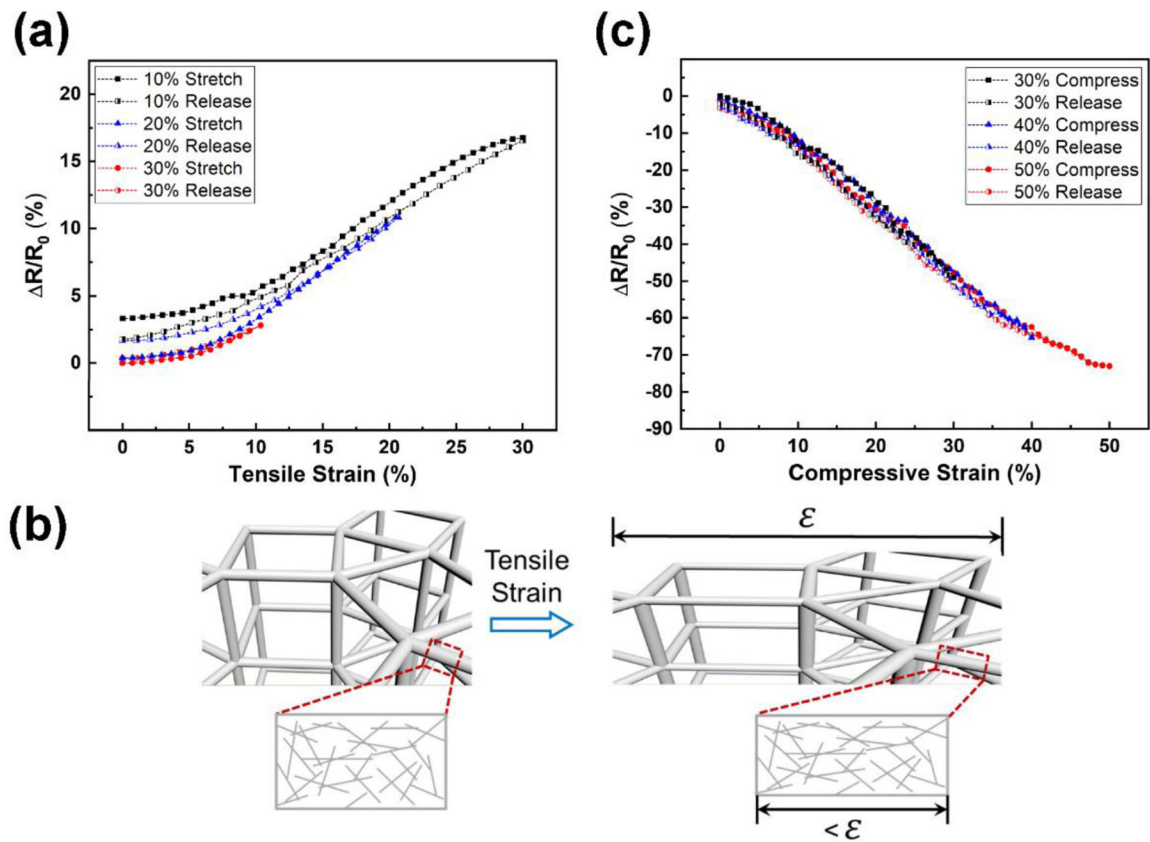
Figure 4.
Mechanical robustness of porous dry electrodes. (a) Resistance changes as a function of tensile strain. (b) Schematics of the binary conductive network under tensile strain. (c) Resistance changes as a function of compressive strain.
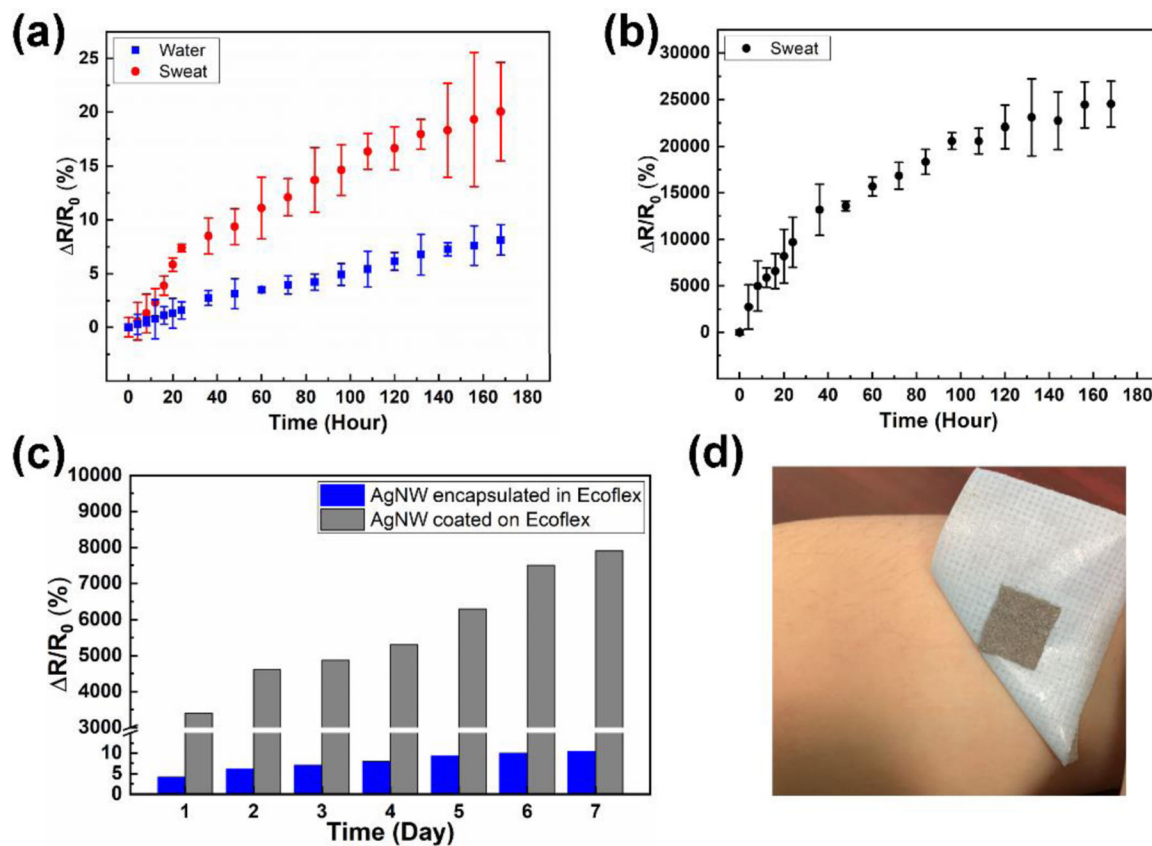
Figure 5.
Stability of porous dry electrodes. (a) Resistance changes over time for porous AgNW/ Ecoflex electrodes immersed in water and sweat. (b) Resistance changes over time for porous electrodes with AgNWs coated on the surface of Ecoflex immersed in sweat. (c) Comparison of resistances changes for electrodes with AgNWs encapsulated in Ecoflex and electrodes with AgNWs coated on the surface of Ecoflex. Electrodes were worn on the skin for 7 days. (d) Photographs of the porous AgNW/Ecoflex electrodes on skin before and after peeling off the electrodes after wearing for 7 days. A breathable medical tape was used for skin attachment.
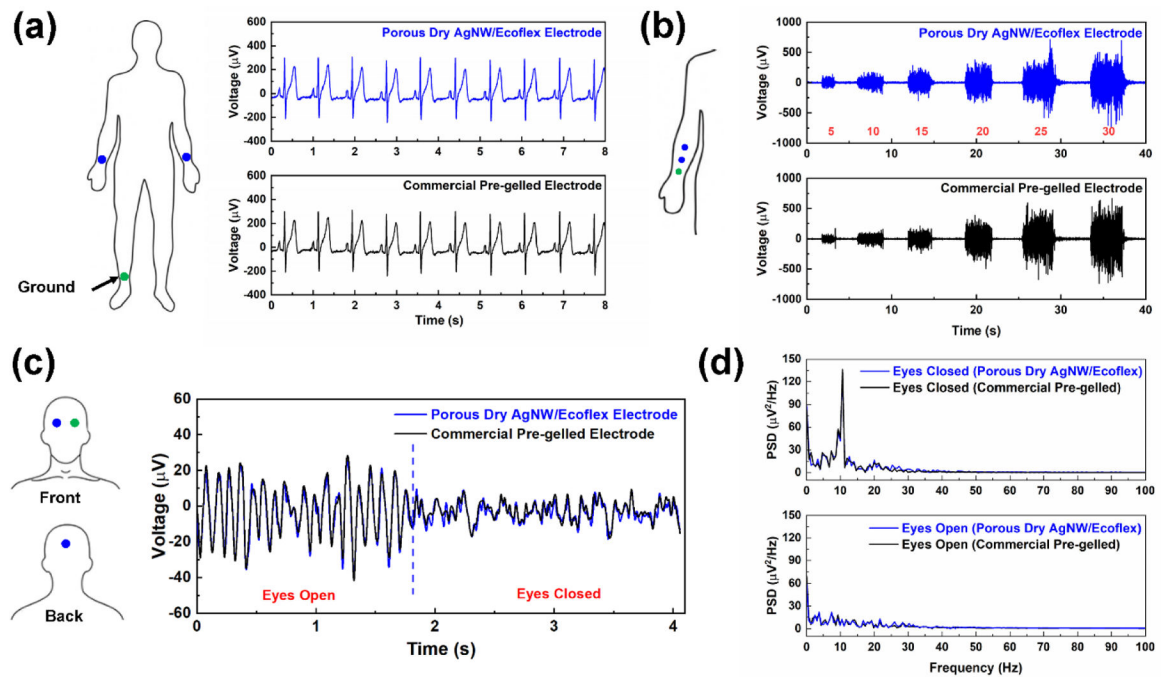
Figure 6.
Applications in biopotential sensing. (a) ECG signals collected from porous dry AgNW/Ecoflex electrodes and commercial pre-gelled Ag/AgCl electrodes. (b)-(c): EEG signals and corresponding PSD spectrograms for porous dry AgNW/Ecoflex electrodes and commercial pre-gelled Ag/AgCl electrodes. (d) EMG signals collected from porous dry AgNW/Ecoflex electrodes and commercial pre-gelled Ag/AgCl electrodes. Grip strength was measured using a dynamometer.
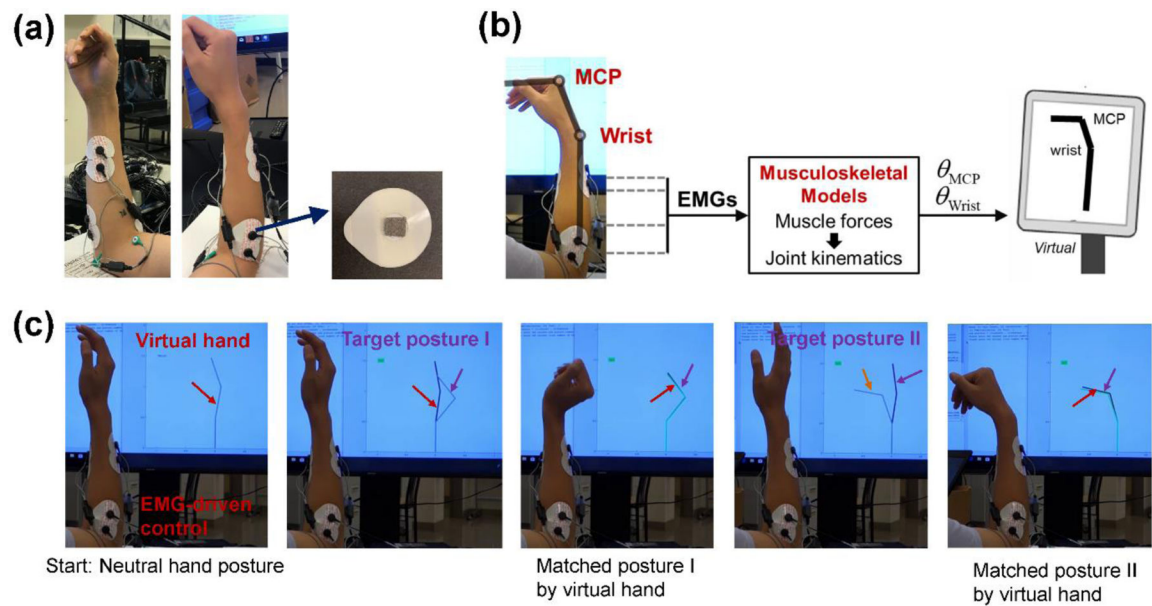
Figure 7.

Applications in EMG-based NMIs. (a) Placement of the surface EMG electrodes on the forearm. The conductive gel in commercial pre-gelled electrodes was replaced with the developed porous AgNW/Ecoflex electrodes. (b) Schematic illustration of real-time EMG-driven control of a virtual hand/wrist based on musculoskeletal models. (c) Images showing the successful matching for different task postures. When the posture of the EMG-controlled virtual hand matches the target posture, the virtual hand turns green to provide visual feedback.

Table 1.

Comparisons of SNRs of ECG/EMG/EEG signals collected from porous dry AgNW/Ecoflex electrodes and commercial pre-gelled Ag/AgCl electrodes.

	ECG	EMG	EEG
Porous dry AgNW electrodes	24.57 dB	24.50 dB	6.39 dB
Pre-gelled electrodes	24.51 dB	25.55 dB	6.45 dB